Journal Title
XX(X):1–14

DOI: 10.1177/ToBeAssigned
www.sagepub.com/

Decoupling of Consecutive GCAI Combustion Cycles by FPGA Based Real-Time Cylinder Pressure Analysis

Maximilian Wick[1], Bastian Lehrheuer[2], Thivaharan Albin[3], Jakob Andert[1] and Stefan Pischinger[2]

Abstract

Gasoline Controlled Auto Ignition (GCAI) combustion offers high potential for CO_2 emission reduction, but faces challenges regarding combustion stability and high sensitivity to changing boundary conditions.[1] Combustion chamber recirculation allows a wide operation range, but results in a strong coupling of consecutive cycles[2] due to residuals that are transferred to the subsequent combustion cycle. The cycle coupling leads to phases of unstable operation with reduced efficiency and increased emission levels.[3] State of the art control algorithms use data-driven models of GCAI combustion to achieve cycle-to-cycle control of the process[4] or use offline calibration and optimization.[5]

A closed-loop control is proposed and implemented on a rapid control prototyping ECU. The control algorithm continuously calculates the current residual fuel in the combustion chamber. The heat release is observed and compared with the theoretical heat release of the injected fuel mass. The rate of unburned fuel mass transferred to the subsequent cycle is calculated offline by a detailed gas exchange model. Based on this information, the control algorithm adapts the injected fuel quantity for each cycle individually using an inverse injector model.

In this article, a concept for decoupling consecutive cycles is presented to reduce the deviations of the indicated mean effective pressure (IMEP) and thus the heat release. Unstable sequences are analyzed in the time domain, and unburned residuals are identified as a strong correlating factor for consecutive cycles. Using real-time cylinder pressure analysis based on a field programmable gate array (FPGA) enables the online calculation of unburned residual fuel. Based on this calculation, the injection of each cycle can be adapted individually to decouple consecutive cycles and avoid unstable operation.

The results of the control algorithm and the stabilization of the GCAI combustion are validated using a single cylinder research engine and compared to steady state operation.

Keywords

Gasoline Controlled Auto Ignition (GCAI), Homogeneous Charge Compression Ignition (HCCI), Field Programmable Gate Array (FPGA), Cylinder-Pressure-Indication, In-Cycle Control

Introduction

Gasoline Controlled Auto Ignition (GCAI) offers a high potential to reduce fuel consumption, comparable to state-of-the-art lean stratified combustion. Furthermore, nearly all NO_x raw emissions can be avoided due to the low combustion temperature.[6,7,8,1] This feature makes GCAI combustion interesting as a way to comply with current and future emission legislation without expensive exhaust gas aftertreatment systems. The decrease in NO_x-emissions and the increase in efficiency compared to conventional stoichiometric operation can be seen in Figure 1. Even in stoichiometric GCAI operation, which is needed at higher loads to comply with emission legislation using a three-way catalytic converter, significant decreases in emissions and fuel consumption can be found.

Operation of the engine at the stability limit of GCAI combustion results in stochastic cycles with incomplete combustion that cannot be predicted precisely.[9] These initial outliers result in characteristic sequences of unstable operation.[10] Cycles with incomplete combustion lead to a significant amount of residual fuel in the exhaust gas which then is partially transferred to the subsequent cycle.[11] Even in multi-cylinder engines this effect is dominant compared to cylinder to cylinder influences.[12] With a constant fuel quantity injected in the following cycle, the total fuel mass increases unintentionally, while the other control parameters such as valve timing or injection timing remain constant.[3] This behavior is also described in Hellström et al.[13]

This work analyses combustion sequences at different load points as well as the effect of residual fuel on the occurrence of unstable sequences in GCAI combustion. A control algorithm for the decoupling of unstable sequences

[1]Mechatronic Systems for Combustion Engines RWTH Aachen University, Aachen, Germany
[2]Institute for Combustion Engines RWTH Aachen University, Aachen, Germany
[3]Institute of Automatic Control RWTH Aachen University, Aachen, Germany

Corresponding author:
Maximilian Wick, Mechatronic Systems for Combustion Engines RWTH Aachen University, Forckenbeckstraße 4, Germany
Email: wick_m@vka.rwth-aachen.de

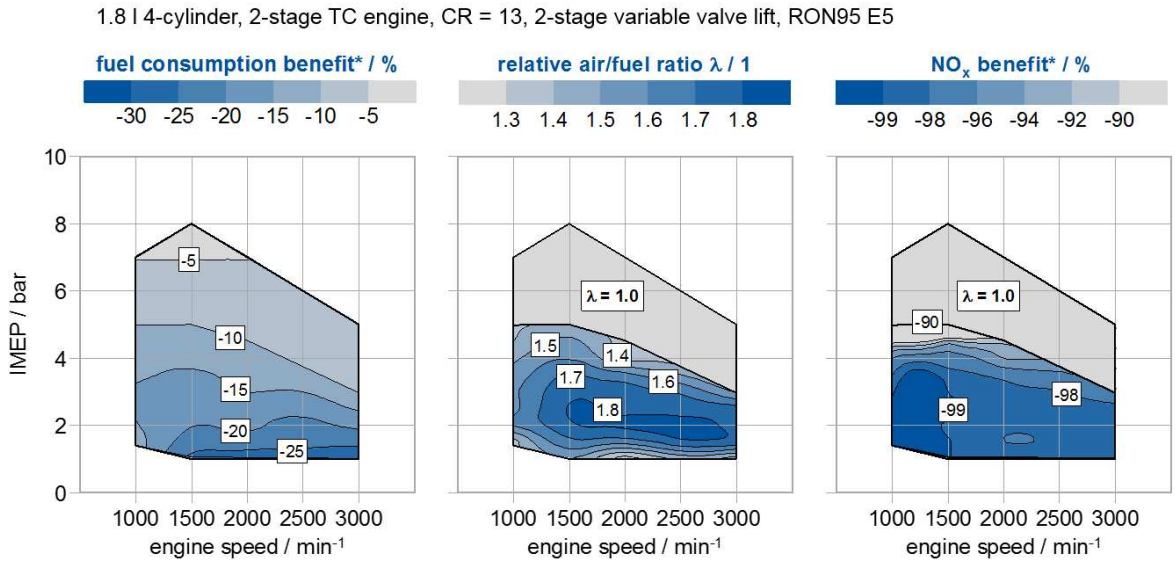

Figure 1. Reduction of fuel consumption and NOx over GCAI operation map

and reduction of high pressure gradients of subsequent cycles is developed and control results are presented. The target of the control strategy is to minimize the impact of stochastic outliers and to achieve stabilized operation of the engine with a constant IMEP.

Motivation

State-of-the-art closed-loop cycle-to-cycle combustion controllers focus on the control of integral substitutes for the combustion, such as IMEP or 50 % heat release angle, α_{50}. In this article, an instantaneous decoupling of consecutive cycles through in-cycle interventions is examined. These in-cycle interventions are only beneficial in certain situations, such as at incomplete combustion or misfire. Characteristic patterns, which occur for example after incomplete combustion, should be interrupted within the same cycle. This interruption helps to avoid phases of unstable and inefficient operation, but it does not replace a global combustion control, which optimizes the stationary operation of the engine. The control interventions cannot be achieved by state-of-the-art cycle-to-cycle combustion control, because they require several cycles for restabilization. Therefore, the decoupling controller is proposed as an add-on to the global combustion control.

The bifurcative behavior in Figure 2 which describes the characteristic pattern was described in Hellström et al.[14] As seen in the diagrams with lower rates of residual gas, the instability of the combustion increases as the range of heat release and the combustion timing varies more. It can also be seen that the maximum of the heat release rises with lower exhaust gas recirculation. Because the injection timing and duration remain constant, the only reason for the higher heat release can be fuel, which is transferred to the subsequent cycle due to the exhaust gas recirculation. The fuel mass was chosen for the decoupling the consecutive cycles because of the detected correlation between incomplete combustion and overshoot in the heat release and IMEP of the subsequent cycle. **Compared to the work of Davis et al.[3] the controller shall focus on a physical approach rather than pure correlation to combustion process substitutes.**

Increasing the residual gas fraction can improve combustion stability but lead to earlier combustion phasing, which is suboptimal for efficiency.[2] Additionally, the gradient of the pressure trace increases with higher residual gas fractions, which leads to higher noise emissions or even engine damage.

The hypothesis of this works is that the sequences are caused by unburned residuals of stochastic misfire cycles. Measures to decouple subsequent cycles will be analysed by engine test bench measurements. A possible solution to avoid unstable operation is to reduce the injected fuel mass of the subsequent cycle by the amount of transferred unburned fuel.

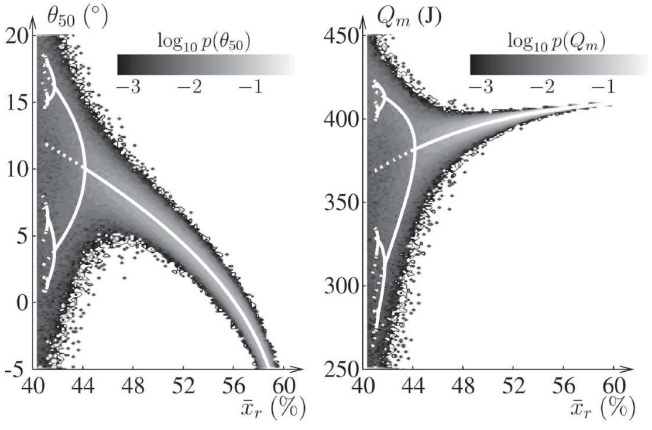

Figure 2. Orbit diagram of the birfucative behavior of GCAI with varying fractions of exhaust gas according to Hellström[14]

Experimental Setup

The investigations are performed on a single-cylinder research engine (SCRE) with a fully variable electromechanical valve train (EMVT) directly controlled by the Field Programmable Gate Array (FPGA) on the prototyping engine control unit ECU. This setup makes it possible to operate

the engine in a wide GCAI operation range with various residual gas strategies such as combustion chamber or exhaust port recirculation. All the measurements in this paper were performed using combustion chamber recirculation. The research engine and the electromechanical valve train used are shown in Figure 3.

The injection system is equipped with a piezo-electrically actuated, outwards-opening hollow cone injector in central position, which is directly actuated by the FPGA. The fuel pressure is set to 100 bar. The geometric compression ratio of the SCRE can be adapted and is set to CR = 12. The test bench is equipped with a temperature conditioning unit that regulates the oil and water temperature to 90 °C. The intake air is conditioned at 50 °C upstream of the intake valves. The experiments are performed with conventional European RON 96 gasoline containing 10 % ethanol. For GCAI operation the throttle is fully opened.

The real-time decoupling algorithm runs on a prototyping ECU with an FPGA (Xilinx Kintex-7) in parallel with the online cylinder pressure indication and the angular computation unit. The thermodynamic postprocessing of the cylinder pressure, measured by a piezoelectrical pressure transducer (Kistler A6061B) is calculated with a resolution of 0.1 °crank angle. For the pressure referencing of the relative pressure measurement, a thermodynamic zero-point correction is performed. The implementation of the cylinder pressure indication on an FPGA is presented in Pfluger et al.[15] The timing of the injection, ignition and the EMVT actuation is directly controlled by the FPGA, so that all actuators can be controlled with the sample rate of 12.5 ns and without additional communication delay. Further boundary conditions and engine parameters can be found in tables 1 and 2.

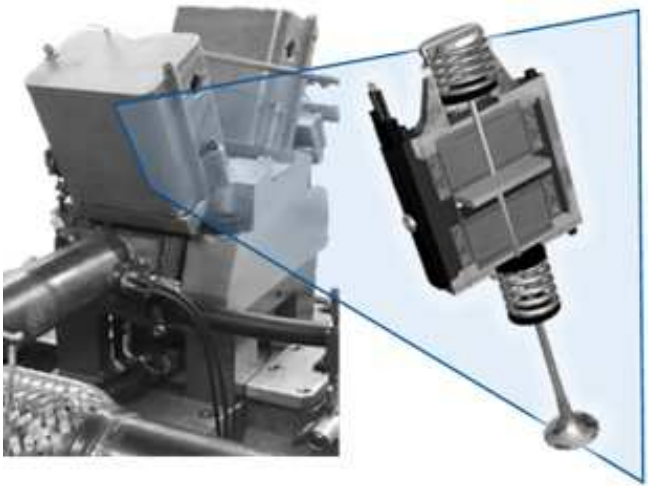

Figure 3. Single cylinder research engine with electromechanical valve train

Table 1. Single Cylinder Research Engine Parameters

Displaced Volume	499 ccm
Stroke	90 mm
Bore	84 mm
Compression Ratio	12:1
# of Valves (In/Ex)	2/2
Valve Train	EMVT
Valve Lift (In/Ex)	8 mm / 8 mm
Valve Angle (In/Ex)	22.5 / 22.5 °
Valve Diameter (In/Ex)	32 mm / 26 mm
Intake Air Pressure	1013 mbar
Exhaust Pressure	1013 mbar
Oil & Coolant Temp.	90 °C
Engine Speed (n)	1500 1/min
Rail Pressure	100 bar
Intake Temperature	50 °C

Table 2. Fuel data

Research Octane Number (RON)	96
Motor Octane Number(MON)	85.8
Upper Calorific Value ($H_{u,Gasoline}$)	44.31 MJ/kg
Ethanol Mass Fraction	10.4 %
Water	360 mg/kg
Density at 20 °C	745.8 kg/m^3
Fuel Temperature	25 °C

Analysis of Combustion Sequences

The combustion phasing correlogram is a useful tool to identify characteristic combustion sequences triggered by stochastic outliers. For a better understanding of the characteristic pattern, the effect of a spontaneous and unpredictable late and incomplete combustion is evaluated in Figure 4. The first outlier, an incomplete combustion that triggers the characteristic pattern, can be seen as a jump from the center of the correlogram to the middle upper side, which represents a late combustion.

The late and incomplete combustion leads to higher exhaust gas temperatures and higher amounts of residual fuel in the exhaust gas. Because of the negative valve overlap (NVO), the hot exhaust gas and the residual fuel are partially transported to the next cycle. In the intermediate compression, further oxidation of the residual fuel can occur, which further increases the exhaust gas temperature. The combustion of the subsequent cycle therefore starts very early and with a high pressure gradient.[10]

This effect is characterized by a jump to the lower right corner of the correlogram, representing the area of early combustion of the actual cycle and late combustion of the previous one. Afterwards, a characteristic pattern of several cycles with early combustion phasing and a high pressure gradient occurs.[10] The restabilization of the combustion process corresponds to the path from the lower left corner (early combustion phasing of the actual and the previous cycle) back to the center of the correlogram.

For a deeper analysis of unstable sequences, the autocorrelation of heat release is analyzed in detail.

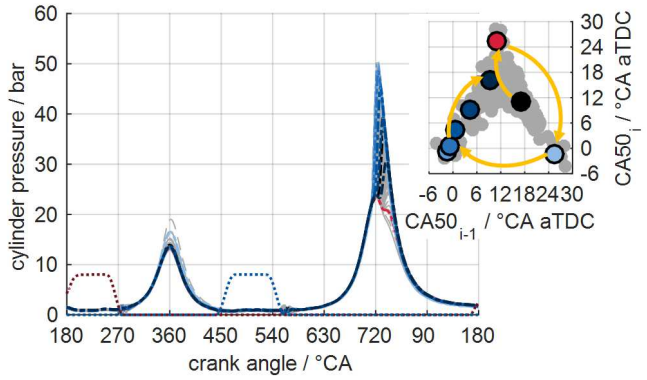

Figure 4. Patterns in consecutive combustion cycles, n = 1500 1/min, IMEP = 4 bar according to Lehrheuer et al.[1]

Calculation of Heat Release

In the thermodynamic analysis, the energy balance is analyzed based on a single-zone model for the combustion chamber. The first law of thermodynamics which describes the change in internal energy dU, is used to calculate of the derivative heat release dQ_B. The calculation is based on the thermodynamic work $-pdV$ and the wall heat losses dQ_W for which a suitable model needs to be found.

$$dU = -pdV + dQ_B - dQ_W \tag{1}$$

For the analysis of the heat release, it is useful to express the change in heat release dU with respect to constant mass and ideal gas. The resulting formula for the derivative heat release dQ_B is calculated using the heat capacity ratio κ, the actual cylinder volume $V(\phi)$, and the measured and referenced cylinder pressure $p(\phi)$. **For the analysis performed in this paper κ was assumed to be constant**:

$$dQ_B = \kappa/(\kappa-1)p(\phi)dV + 1/(\kappa-1)V(\phi)dp + dQ_W \tag{2}$$

The derivative wall heat transfer dQ_W depends on the surface including terms of the current crank angle ϕ, the heat release coefficient and the temperature difference between the combustion chamber and the combustion wall. The temperature in the cylinder $T_{Cyl}(\phi)$ is approximated by the ideal gas law, and the temperature of the wall T_{Wall} is assumed to be constant ($T_{Wall} = 400\,\mathrm{K}$) for the shown operation point:

$$dQ_W = \alpha(\phi)A(\phi)(T_{Cyl}(\phi) - T_{Wall}) \tag{3}$$

For the estimation of the heat transfer coefficient $\alpha(\phi)$, multiple approaches are presented in the literature. In this paper the Hohenberg approach[16] is implemented to calculate of the heat release. This approach is commonly used for direct injection diesel engines, but it also suits GCAI combustion very well because of the high pressure gradient:[17]

$$\alpha(\phi) = 0.013V(\phi)^{-0.06}p(\phi)^{0.8}T(\phi)^{0.4} \\ (v_{Piston} + 1.4)^{0.8} \tag{4}$$

The integration of the derivative heat release is performed for a fixed range of crank angle. An individual-cycle calculation starting with the detected beginning of the combustion is not suitable, because of the need to detect incomplete combustion and even misfire.

While analyzing the combustion pattern, a conversion of fuel in the intermediate compression was also found, especially at higher load points above 2 bar. Because of the possible conversion of residual fuel in the intermediate compression two heat releases are calculated, one in the main combustion and another one in the intermediate compression. The heat release in the main combustion is integrated from 45° CA bTDC to 90° CA aTDC. In the intermediate compression, the integral is calculated symmetrically to the gas exchange TDC (310°to 410° CA aTDC).

$$Q_{\mathrm{B,Comb}} = \int_{-45°CAaTDC}^{90°CAaTDC} dQ_B d\phi \tag{5}$$

$$Q_{\mathrm{B,GE}} = \int_{310°CAaTDC}^{410°CAaTDC} dQ_B d\phi \tag{6}$$

Heat Release Correlation Analysis

Different load points at a speed of 1500 1/min are examined in the steady-state condition. To establish good statistical significance, measurements for 200 combustion cycles are used in the analysis. The characteristic outlier is defined as the cycle with the lowest heat release in the main combustion in the overall measurement. Starting from that cycle, the behavior of the previous two and following three cycles is investigated. For that analysis, correlograms of the heat release during the main combustion are plotted in Figures 5, 6 and 7 for different load points.

First, a measurement with an average load of IMEP = 3.4 bar is shown in Figure 5a. The y-axis shows the current heat release in the main combustion, while the x-axis represents the previous cycle's characteristics. The outlier cycle with the lowest heat release is marked in the lower area of the heat release correlogram. The position in the lower middle part of the correlogram means that the actual cycle has a low heat release while the previous one had an average one. This observation underlines that the prediction of a spontaneous incomplete combustion is very difficult, and minimization of the effects is required.

That cycle is followed by a slightly above-average heat release in the left area of Figure 5. The heat release after incomplete combustion is 540 J, higher than average the of ca. 520 J but within the standard deviation of the heat release. The high exhaust gas enthalpy at higher loads leads to oxidation of the residual fuel during intermediate compression. As a consequence, the heat release of the subsequent combustion corresponds to the injected fuel amount because no residual fuel remains.

The lower part of Figure 5 illustrates the IMEP development. For this work the IMEP is calculated from 180° CA before firing TDC to 540° CA after firing TDC. Consequently, the combustion during intermediate compression is imputed to the same injected fuel mass as

the prior combustion. It can be seen that the IMEP of outlier cycle 87 is very low and the IMEP of the subsequent cycle 88 is only slightly above average. No overshoot of the heat release nor the IMEP due to unburned residuals is evident.

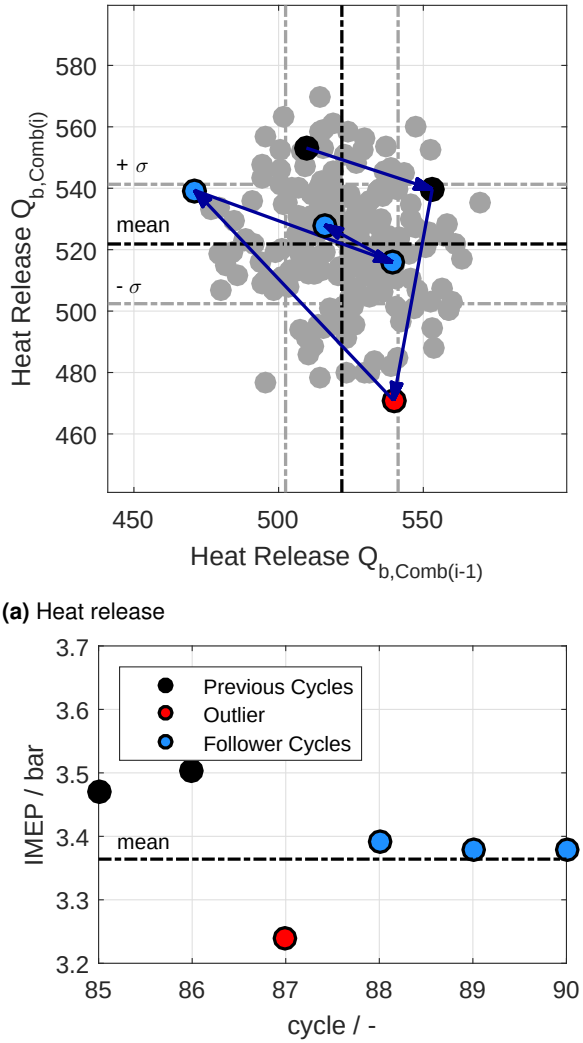

(a) Heat release

(b) IMEP

Figure 5. Analysis of heat release for consecutive cycles at n = 1500 1/min and IMEP = 3.3 bar

Decreasing the load to IMEP = 2.2 bar reveals a different behavior (Figure 6). The stochastic outlier with an incomplete combustion occurs at cycle 28. The IMEP was decreased by 0.5 bar to 1.7 bar at that point. The subsequent cycle has an IMEP of 2.7 bar, an increase of 23 % compared to the mean value.

In the same manner, the heat release increases approximately by 28 % to 440 J. The trace of the subsequent cycles in the correlogram forms a characteristic triangle that can also be found at lower loads.

Figure 7 shows the same diagrams for a lower load of IMEP = 1.6 bar which represents the misfire limit of the SCRE with GCAI combustion.

The incomplete combustion is detected in cycle 157 and represented by a heat release below 150 J and an IMEP below 1 bar. The subsequent cycle exceeds the average values of both heat release and IMEP significantly. Here, the residual fuel is not necessarily converted during intermediate compression and leads to an increased amount of fuel

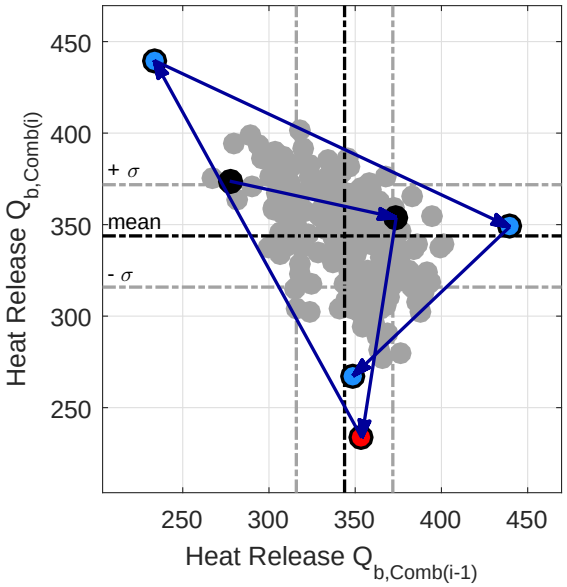

(a) Heat release

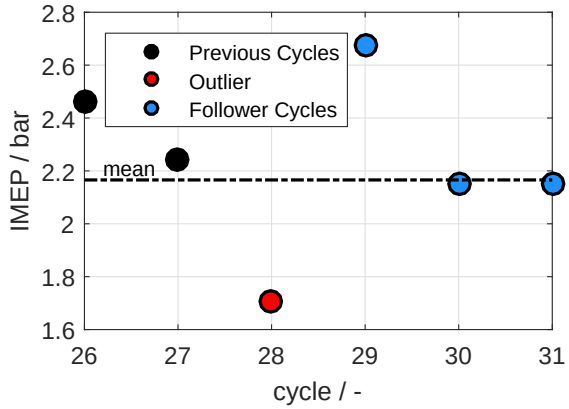

(b) IMEP

Figure 6. Analysis of heat release for consecutive cycles at n = 1500 1/min and IMEP = 2.2 bar

and thus to a higher heat release during the subsequent combustion (Figure 7a). **This observation differs to the one Jade, S. et al[18] made with a multicylinder engine, where all fuel is burned in the intermediate compression.**

The analysis of the combustion pattern shows significant correlations between incomplete combustion and the overshoot in IMEP and heat release at lower loads. The position of the following cycle in the correlogram is important for the control results. The farther left the point is in the correlogram, the better it can be detected. The height of the point suggests the opportunity to influence that cycle by an adapted injection.

At loads above 2 bar IMEP, this correlation cannot be directly observed. Characteristic sequences with overshoot in heat release or IMEP have not been identified. Therefore, higher loads of IMEP greater than 2 bar do not seem to be promising for an active decoupling algorithm through adaption of the fuel mass.

Loads below 2 bar IMEP show an overshoot in the heat release and IMEP of more than the standard deviation of that measurement. A decoupling control algorithm (DCA) to influence the heat release of the subsequent cycle based

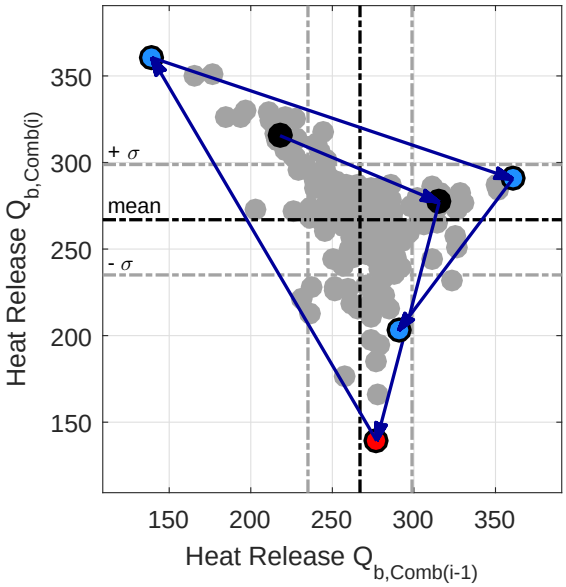

(a) Heat release

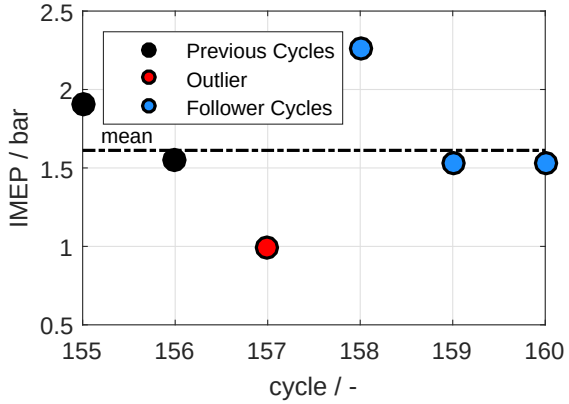

(b) IMEP

Figure 7. Analysis of heat release for consecutive cycles at n = 1500 1/min and IMEP = 1.6 bar

on the prediction of IMEP overshoot is proposed in the following section.

Decoupling Control Algorithm

To avoid an unstable combustion pattern the subsequent cycle must be decoupled from the prior incomplete combustion. Since the residual fuel is believed to be the main reason for the overshoot in IMEP and heat release, decoupling is possible through adjusting the injected fuel mass by the amount of residual fuel transferred to the subsequent cycle.

In the following sections, the main steps for the calculation of the residual fuel, the prediction of IMEP and the adapted injection timing are explained. All of the calculations are then integrated on the FPGA part of the prototyping ECU for online control interventions. Timing and hardware constraints will also be explained.

Estimation of Residual Exhaust Gas

One major influencing factor for the characteristic pattern described above is the residual fuel transferred to the subsequent cycle. The unburned fuel is divided into a part that leaves the combustion chamber through the exhaust port and another part that stays inside the combustion chamber. For the decoupling controller, the assumption was made that the amount of fuel trapped inside the combustion chamber directly correlates with the fraction of the exhaust gas.

To estimate of the fraction of residual gas trapped inside the combustion chamber, a 1D-gas exchange simulation is used for all load points. The model includes all intake and exhaust manifolds and is calibrated with measurement data. The resulting fraction of exhaust gas recirculation was assumed to be constant for each load point and independent of cyclic fluctuations.

To validate the assumption that the exhaust gas fraction is constant, CFD-simulations including cyclic fluctuations were performed in Morcinkowski et al.[19] Figure 8 compares measured and simulated results. It can be seen that the simulation covers the variety of cyclic fluctuations over several cycles.

Figure 8. Fluctuations of GCAI-Combustion in measurement and simulation according to Morcinkowski et al.[19]

Figure 9 shows that the simulation results also cover the cyclic fluctuations of the combustion process, and no dependency of the exhaust gas fraction can be found.

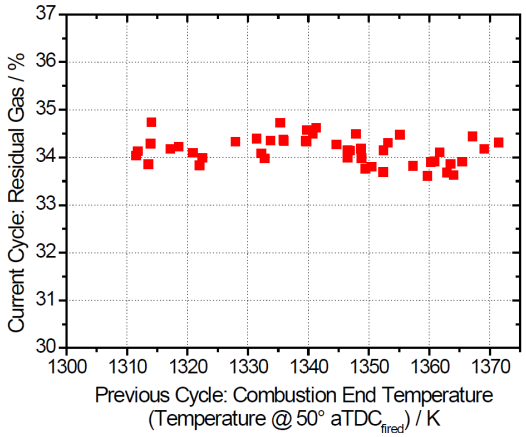

Figure 9. Dependency of exhaust gas fraction on cyclic fluctuations according to Morcinkowski et al.[19]

Calculation of Residual Fuel

The amount of residual fuel is believed to be the main parameter influencing the overshoot of the heat release and IMEP and therefore must be calculated as accurately as possible. To calculate the residual fuel, exact knowledge of the injected fuel mass as well as the burned fuel mass is required.

In the intermediate compression, another conversion of residual fuel can occur. Therefore, the amount of fuel burned during the intermediate compression needs to be considered when calculating the amount of fuel transferred to the next combustion cycle. Combining all previous information the following equation for the calculation of the residual fuel transferred to the next cycle can be found:

$$m_{\text{fuel,res}} = (m_{\text{fuel,inj}} - m_{\text{burned,Comb}})x_{\text{Egr}} - m_{\text{burned,GE}} \quad (7)$$

The first step is to estimate the injected fuel mass using a detailed injector model. For that purpose, the following dazzle equation is used:

$$m_{\text{fuel,inj}} = \alpha \cdot A\sqrt{2 \cdot \varrho \cdot \Delta p} \cdot t_{inj} \tag{8}$$

The non-linear opening and closing behavior of the used piezo injector is taken into account by adapting the flow coefficient α over the injection duration (DOI). The calibration of the model is performed with multiple measurements at an injection test bench as well as on the SCRE. It can be seen that with a higher injection duration, the influence of the non linearities diminishes. At low load points with short injection duration this effect cannot be neglected. Due to the controller targeting the control of low load points with short injection duration, a precise estimate of the effect of adapting the injection duration is necessary.**To avoid unstable behavior of the controller the control algorithm has to be robust against changing boundary conditions[20] as for example charge cooling.**

The results of the calibration of the injector model on the injection testbench can be found in Figure 10. The fuel pressure is kept constant at 100 bar, and the start of injection timing corresponds to the opening of the intake valves at unthrottled operation (cp. table 1). Therefore, the pressure difference between the fuel rail and the cylinder Δp is almost constant and can be low-pass filtered because no individual cycle effects are expected. The fuel density ϱ was measured in a detailed chemical analysis of the used RON 96 fuel and is 745.8 kg/m^3.

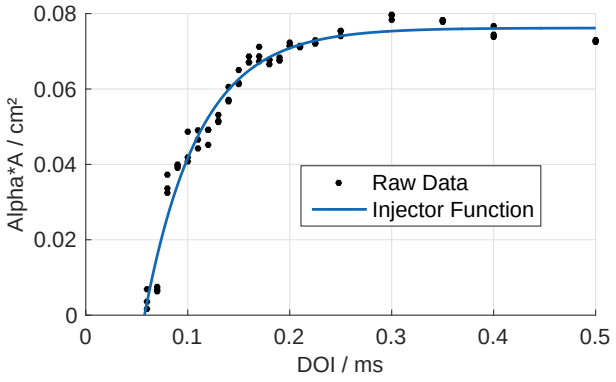

Figure 10. Correlation of injection timing, flow coefficient and injector cross-section

As shown before, the heat release is calculated in two intervals, during the main combustion and during the intermediate compression. With the knowledge of the total heat release in the two different stages of the combustion cycles, the burned fuel mass for both intervals can be calculated using the upper caloric value of the used fuel.

$$m_{\text{burned,Comb}} = \frac{Q_{\text{B,Comb}}}{H_{\text{u,Gasoline}}} \tag{9}$$

$$m_{\text{burned,GE}} = \frac{Q_{\text{B,GE}}}{H_{\text{u,Gasoline}}} \tag{10}$$

To validate the online calculation and the implemented injector model measurements with constant injection timing are performed. The results for the calculated injected, burned, and residual fuel mass for 200 cycles in steady-state operation at 1500 1/min and IMEP = 1.6 bar are shown in Figure 11. The measurement shows several outliers with incomplete combustion. Due to negligible conversion in the intermediate compression the incomplete cycles can also be found in the residual fuel.

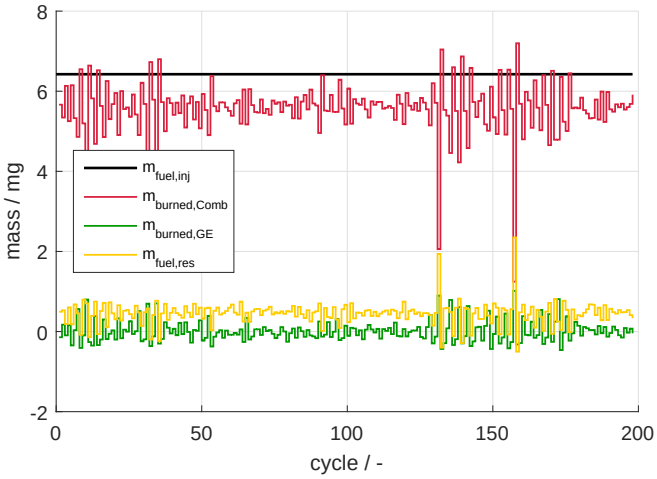

Figure 11. Calculated fuel mass for 200 consecutive cycles

Prediction of IMEP

To validate the assumption that the fuel mass is the main influencing factor for overshoots in IMEP and heat release, an offline prediction of the IMEP based on the unburned fuel mass is performed.

For the decoupling control algorithm the assumption was made that the efficiency of the combustion process does not depend on the mass of unburned fuel. Thus, any amount of residual fuel leads to the same increase in IMEP. Therefore the prediction is a linear approach with the following equation:

$$\text{IMEP}, i = \text{IMEP}_{\text{target}} \frac{m_{\text{fuel,res},(i-1)}}{m_{\text{fuel,inj}}} + \text{IMEP}_{\text{target}} \tag{11}$$

The gradient of the prediction with DCA is the target IMEP divided by the injected fuel mass as a factor indicating the efficiency. The IMEP of the actual cycle is calculated only with the knowledge of the mass of unburned fuel of the predecessor cycle. The target IMEP and the injected fuel mass remain constant.

A global combustion control without DCA does not predict the IMEP of the following cycle depending on the amount of residual fuel. Therefore, the prediction results are represented horizontal lines at the target IMEP.

The results of the prediction can be seen in Figure 12. The measurement results shown are the same as in the previous analysis of the combustion sequences.

For the load point with 3.3 bar IMEP, only very small amounts of unburned fuel are evident. Therefore, no reliable prediction of the next IMEP with or without DCA can be made. Correspondingly, no significant improvement can be

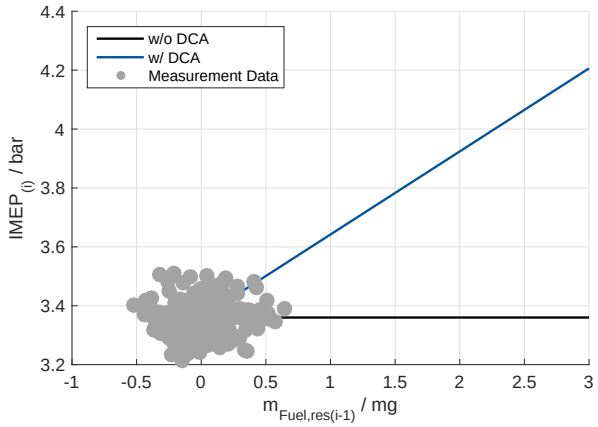

(a) 1500 1/min, 3.3 bar IMEP

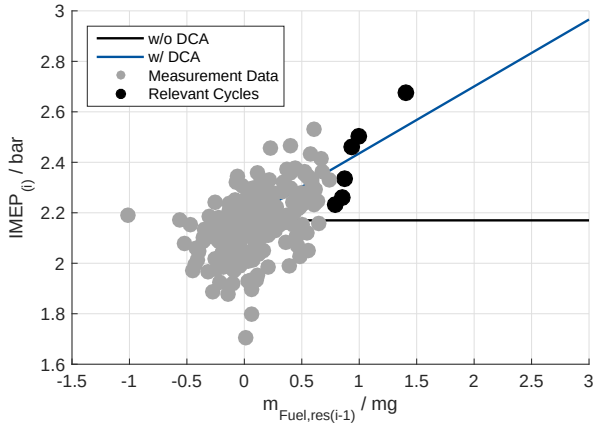

(b) 1500 1/min, 2.2 bar IMEP

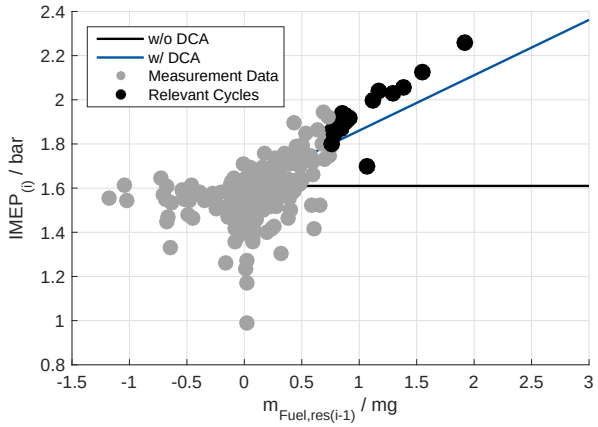

(c) 1500 1/min, 1.6 bar IMEP

Figure 12. Comparison of IMEP prediction results with and without DCA

achieved with DCA. For lower load points it can be seen that the plotted points approach the DCA prediction more and more closely. To avoid the influence of stochastic outliers a threshold of unburned fuel of 0.75 mg was chosen to detect relevant cycles. The relevant cycles that can then be influenced are highlighted in black in the diagrams. Whereas the 2.2 bar operation point has 6 relevant cycles that can be influenced, the 1.6 bar load point already shows 13.

It can be clearly seen that the relevant cycles are closer to the prediction with DCA than without it. To quantify the accuracy of the prediction, the standard deviation of the IMEP prediction $\sigma\Delta\text{IMEP}$ of the relevant cycles is used. For the 2.2 bar IMEP point the standard deviation is 0.3132 bar without DCA, whereas with DCA it would be only 0.1175 bar. The prediction results improve still further with lower load. For the operation point with the lowest load (1.6 bar IMEP), the standard deviation without DCA increases to 0.3707 bar, and the standard deviation with DCA decreases to only 0.1066 bar.

The decreasing standard deviation of the IMEP prediction error with DCA is a good indication that the proposed prediction can be used for the decoupling control algorithm to stabilize the combustion process.

Nevertheless, it can be seen that most of the relevant points are higher than the prediction with DCA, especially at the lowest load point. This error is likely due to the assumption of constant efficiency independent of the residual fuel mass **or the assumption that κ is constant**. Considering this effect could require a further improvement of the control algorithm, but will lead to further calibration effort depending on the load point.

Control Structure

Summarizing the information derived from the analysis and calculation of intermediate results, the control structure of the decoupling control algorithm can be seen in Figure 13.

All of the intermediate results explained above can be found in the structure. Inputs from external sources are marked by arrows, which are calculated in other DCA subsystems. External signals are the cylinder pressure p_{Cyl}, which is measured; the injection duration $t_{\text{injection,i}}$, and the target fuel mass $m_{\text{fuel,target}}$, which are input from the global combustion control. The fraction of exhaust gas recirculation x_{Egr} is simulated offline and saved on the prototyping ECU.

The target of the supposed controller is the calculation of an individual-cycle injection timing that avoids the overshoot in IMEP caused by residual fuel from the preceding cycle. The target fuel mass is reduced by the amount of residual fuel transferred to the subsequent cycle in a last step. The inverted injector model is used to calculate the adapted injection duration to stabilize the combustion process.

A real-time calculation of the unburned fuel mass and an inverted injector model are required. Due to the complex calculation, the use of the FPGA part of the prototyping control unit is beneficial. The DCA code is implemented so that all necessary input data is sampled with a constant angular resolution of 0.1° CA.

Timing Constraints of Online Algorithm

As explained above, the residual fuel mass of the preceding cycle, $m_{\text{Fuel,res}}$, must be taken into account for each injection to avoid any overshoot in IMEP and heat release. To calculate of the residual fuel mass, formula 7 is presented. Part of that formula is the calculation of the burned fuel mass in the intermediate compression which makes timing constraints very difficult because of the short interval between the intermediate compression and the injection.

The duration of the subsequent injection is calculated by the inversion of the injector model presented previously. In Figure 14, the calculation sectors for the heat release in the main combustion and intermediate compression as well as the calculation of the control algorithm are shown.

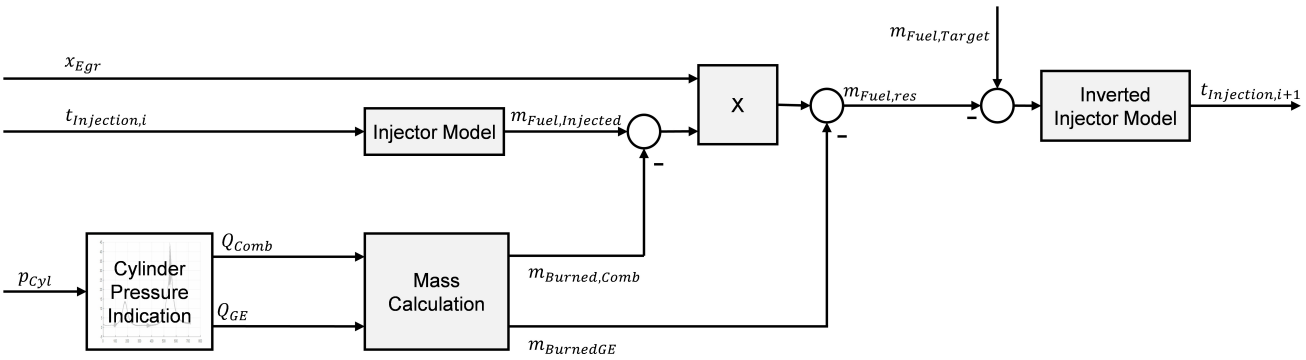

Figure 13. Structure of control algorithm

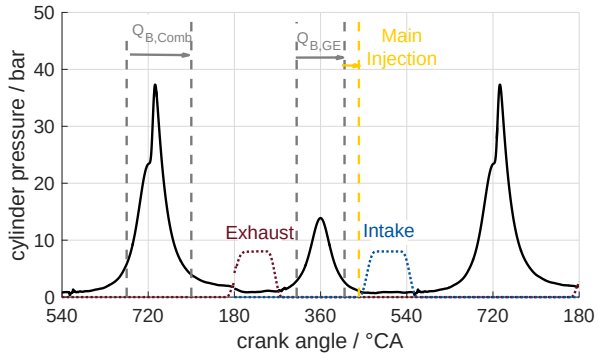

Figure 14. Available calculation time

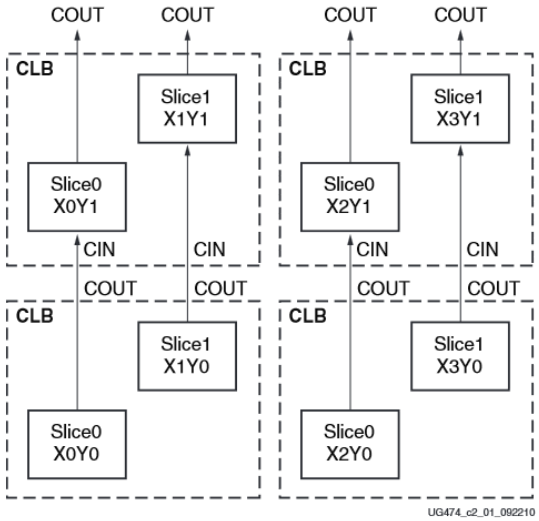

Figure 15. Configurable Logic Blocks (CLBs) with two slices according to Xilinx[21]

Because of the requirement to calculate the heat release in the intermediate compression, the fixed injection timing (EOI at 440° CA aTDC for that load point) and the injection duration of approximately 4° CA, only 26° CA are available for the calculation (marked as the time for the main injection in Figure 14). This value equates to less than 3 ms at an engine speed of 1500 1/min. At higher engine speeds the available calculation time decreases disproportionately. It is clear that the maximum calculation time of the decoupling controller is a very challenging constraint for current RCP hardware.

To achieve this goal, the controller shown in Figure 13 is integrated into the FPGA part of the engine control unit to minimize latency and guarantee real-time constraints.

Hardware Resources

FPGAs consist of configurable logic blocks (CLBs) which include the logical elements of the FPGA in two slices (Figure 15). These basic blocks can be connected individually to implement the programmed code. Accordingly, the load of the FPGA cannot be adjusted by down sampling of the code, but by intelligently considered implementation of control algorithms. Therefore, saving physical space through optimized routing of the FPGA is necessary.

Because of the fast sample rate of 12.5 ns, time sharing of the same algorithm is a common tool for multi cylinder engines. For the single-cylinder engine used, time sharing is not necessary, but the same heat release algorithm (hard-wired connections on the FPGA) is used to calculate the main combustion and the intermediate compression. After calculation, each result is saved in a separate Flip-Flop (FF).

To check the efficient implementation of the decoupling control algorithm, the used space on the FPGA is compared before and after the implementation of the control algorithm. The hardware resources used of the FPGA for the online cylinder pressure indication, including all supporting functions but without the newly developed control algorithm, are shown in table 3. It is not possible to simply compile the code for the decoupling control algorithm separately, because there are cross influences between the connections of the control logic blocks.

The resources used for the code, including all new programmed features, can be seen in table 4.

The comparison shows that there is only a moderate increase of resources for the FPGA. Whereas the Flip-Flops, which are mainly used as memory elements, overall increase by only 3 %, the Lookup-Tables (LUT) as well as the Memory-LUTs have the largest increase because they realize the implementation of the controller. The increase in Block-RAM (BRAM) can be explained by the storage of the calibration data for the injector model. The additional I/O is used for data exchange between the FPGA and the microprocessor side. The Digital-Signal-Processing (DSP48)-Elements are used for common operations such as

Table 3. Hardware Resources of the FPGA without Control Algorithm

Resource	Available	Utilized	Percentage of Use
FF	407600	41756	10.24
LUT	203800	40877	20.06
Memory-LUT	64000	4421	6.91
I/O	478	229	47.91
BRAM	445	58	13.03
DSP48	840	99	11.79
BUFG	32	8	25
PLL	10	3	30

Table 4. Hardware Resources of the FPGA with Control Algorithm

Resource	Available	Utilized	Percentage of Use
FF	407600	55983	13.73
LUT	203800	51312	25.18
Memory-LUT	64000	4832	7.55
I/O	478	233	48.74
BRAM	445	72	16.18
DSP48	840	119	14.17
BUFG	32	8	25
PLL	10	3	30

multiplication without making use of standard elements such as FF and LUTs.

The decoupling control algorithm can easily be extended to multicylinder applications, because due to time-sharing, the same parts of the FPGA can be used within one combustion cycle.

Results

A decoupling control algorithm based on a cyclic adaption of fuel injection was proposed to disrupt the characteristic pattern shown previously in Figure 4. The analysis of the combustion patterns lead to the conclusion that it is possible to interrupt the pattern at loads below 2 bar IMEP using the DCA concept.

The control results of the test bench experiment at n = 1500 1/min and IMEP = 1.8 bar are shown in Figure 16. In the first diagram the pressure traces of five consecutive cycles are shown. With the measured pressure traces from the top diagram the control algorithm can calculate the heat release and the IMEP online.

Heat release and IMEP are shown in the 2nd and 3rd diagram, respectively. Signals are updated according to their specific integration intervals and refer to the past due to causality. The last diagram shows the injection duration which is adapted by the controller. The value for the injection duration that is relevant for the subsequent cycle is highlighted by the circles.

The controller sensitivity was tuned according to the findings of the offline analysis. Only amounts of residual fuel greater than 0.75 mg lead to a control intervention with the injection duration (DOI).

At $t = 0.07$ s, an incomplete combustion is detected. The heat release is significantly lower than the average of the previous cycles. The absolute value of the heat release of that cycle is 189 J, which represents a fuel mass of 4.5 mg compared to an average heat release of 280 J, or 6.6 mg of fuel. The control algorithm decreases the injection time by the corresponding fuel mass, using of the inverted injector model.

Approximately 50 % of the unburned 2.1 mg of fuel is transferred to the subsequent cycle due to exhaust gas recirculation. In the following intermediate compression, a heat release of 39 J is calculated, which means that the residual fuel is converted during intermediate compression. Of the transferred 1.05 mg, another 0.9 mg is burned. The very small amounts of residual fuel left over can be neglected, according to the analysis in the ”Prediction of IMEP” section. Therefore, the control intervention is ended shortly before the main injection.

At $t = 0.22$ s, another incomplete combustion with an even lower heat release (heat release 119 J, 2.83 mg of fuel burned) is detected by the controller. Again the injection duration is reduced by the amount of 1.9 mg (3.8 mg of unburned fuel multiplied by the exhaust gas fraction of 50 %). Because of the low fuel conversion in the subsequent intermediate compression (heat release 45 J, 1.07 mg of fuel burned), an adaption of the fuel mass is still necessary to avoid overshoots in IMEP and the subsequent heat release in the main combustion. The injected fuel mass must be reduced by the transferred fuel mass of 0.83 mg, which is a reduction of the fuel mass by 12.6 %.

It can be seen that at 0.26 s, the injection duration marked by the circle is only 0.24 ms, compared to the 0.28 ms of the target injection duration, which is a reduction by approximately 14 % caused by the non linear injector model. The overshoot of IMEP and heat release in the next cycle is avoided. The control target of 1.8 bar IMEP is maintained.

Two different behaviors of the controller are evident after the time-based analysis of the control algorithm. After an incomplete combustion, the behavior of the control algorithm depends on the fuel conversion during the intermediate compression. If the heat release in the intermediate compression indicates that all of the transferred fuel is converted, it is not possible to influence the next combustion cycle through the DCA. If, on the other hand, there is no or only very little heat release in the intermediate compression, the control algorithm can successfully stabilize the combustion by decoupling the consecutive cycles of the characteristic combustion pattern.

As explained in the heat release correlation analysis the controller should avoid the early combustion after

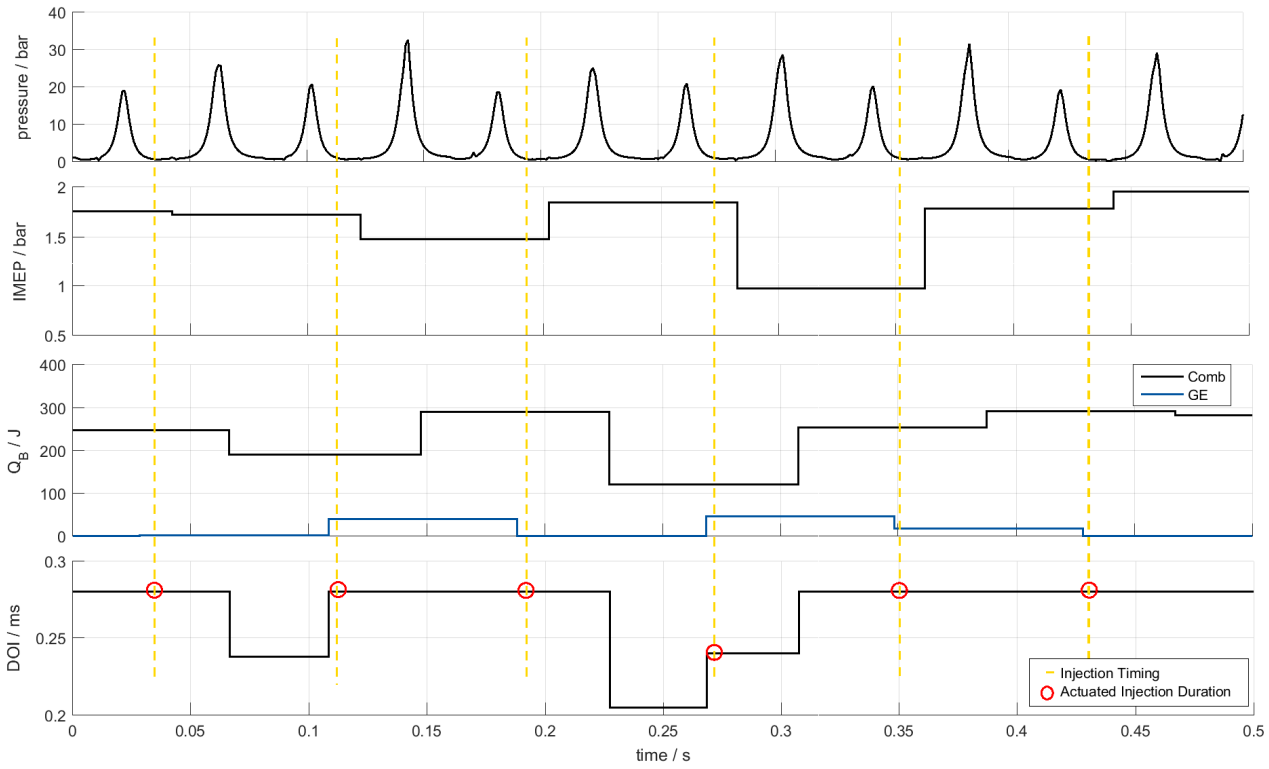

Figure 16. Control impact at n = 1500 1/min and IMEP = 1.8 bar

an incomplete late combustion. In the heat release correlogram this can be seen as a jump from the middle upper half to the lower right corner. In figure 19 the base heat relase correlogram for a load point of 1.7 bar IMEP at 1500 1/min is shown without the decoupling control algorithm. A distinct right arm of the correlogram is visible. As a indication for the combustion stability the standard deviation of the heat release is calculated to 58 J.

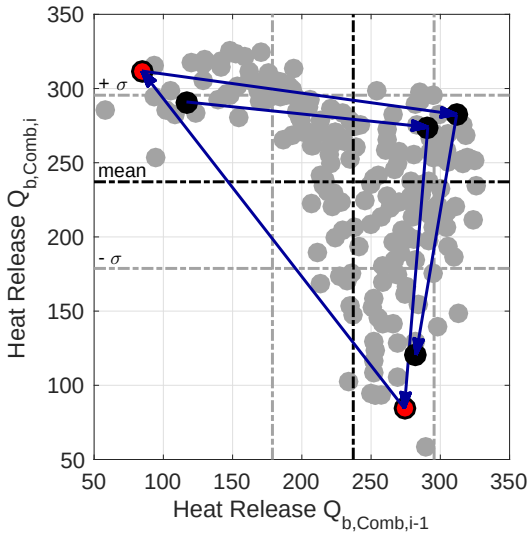

Figure 17. Combustion phasing correlogram without decoupling control algorithm

After activation of the decoupling control algorithm for the same operation point, cycles in the lower left corner of the correlogram are reduced by fuel mass adaption. This leads to an overall stabilization of the combustion. The deviation of the heat release is reduced to 40 J (-31 %). The results can be seen in figure 20

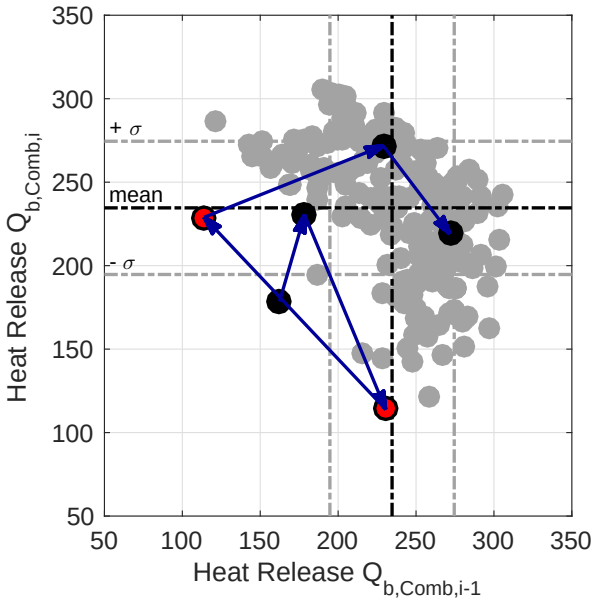

Figure 18. Heat release correlogram with decoupling control algorithm

A suspected deterioration of the combustion phasing because of changing injected fuel mass and combustion efficiency is unfounded, rather combustion phasing should be more stable due to the combustion fuel mass being controlled to stay constant. The survey of the combustion phasing correlogram (figures 19 and 20) is done for the same load point as mentioned above. The upper one without, the lower one with decoupling

control active. The combustion phasing is shifted by only 0.9° CA. Whereas the standard deviation is reduced from 3.8° CA to 2.9° CA (-24 %). This again shows the successful adaption of the fuel mass with the help of the decoupling controller.

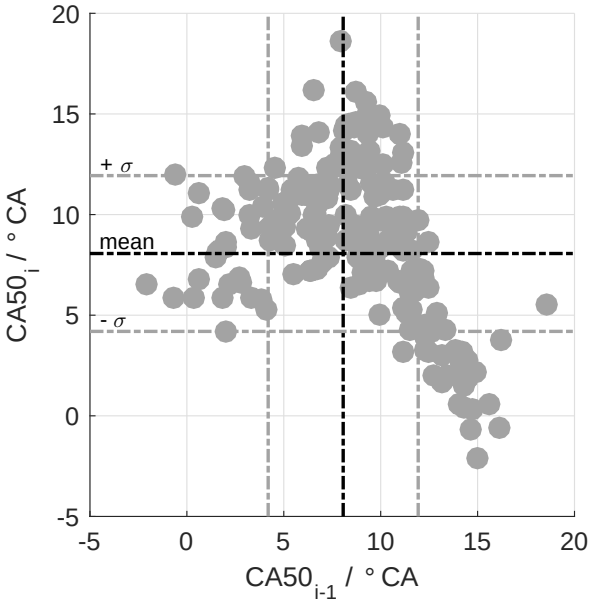

Figure 19. Combustion phasing correlogram without decoupling control algorithm

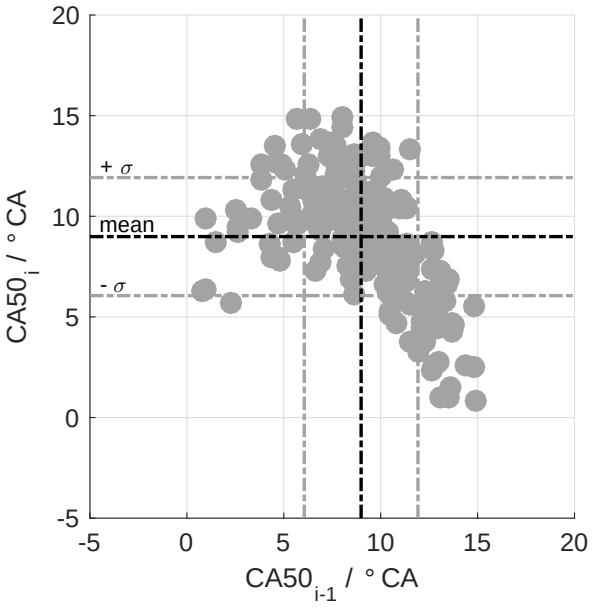

Figure 20. Combustion phasing correlogram with decoupling control algorithm

The introduced prediction correlograms which consider the residual fuel are also a very good tool to analyze control quality. In figure 21 the measurement point used for the investigation of the control interventions, is shown without the controller active. It can be seen that again the IMEP is following the prediction curve. The relevant cycles for the control algorithm are marked in black.

After activation of the decoupling control algorithm the IMEP of subsequent cycles shall not follow the prediction curve but rather stay constant. In figure 22 it can be seen that relevant cycles with a residual fuel mass of more than 0.75 mg lead to actuation of the control algorithm. The cycles are decoupled and following the curve without correlation.

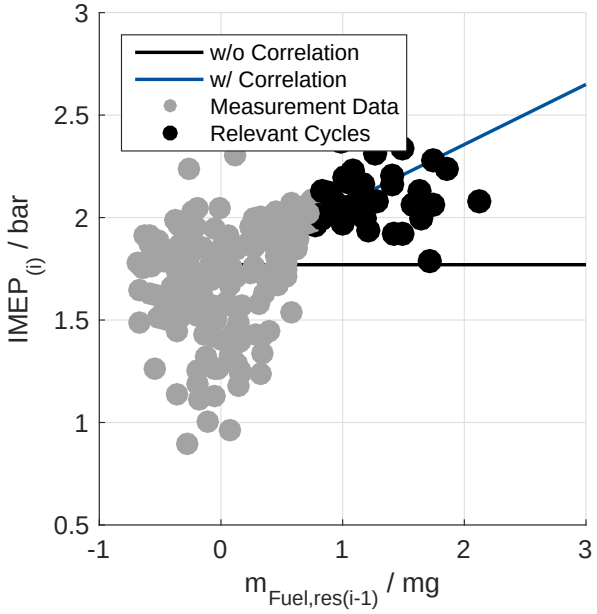

Figure 21. Prediction correlogram without decoupling control

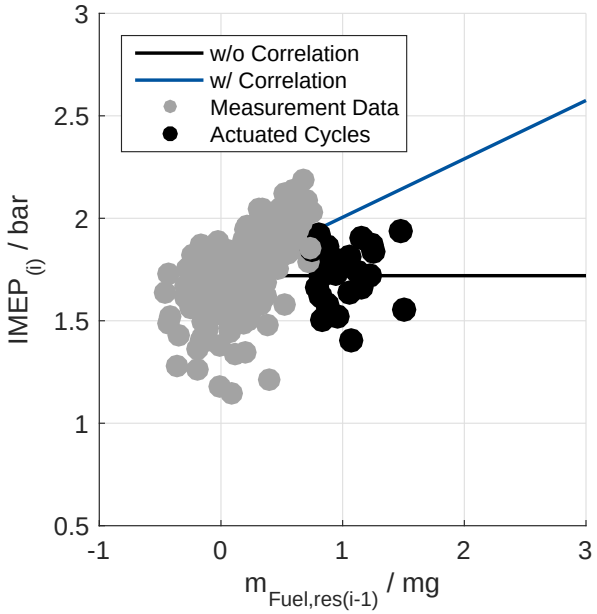

Figure 22. Control results in prediction correlogram

In the next step the control algorithm was tested at slightly different load points to confirm its usability. The results of the stabilization of the combustion can be found in table 5. For each measurement, 250 cycles of steady-state operation are compared to 250 cycles with DCA active. **It can be seen that already a small number of control interventions** in a range of 2/250 to 4/250 **lead to a significant improvement of combustion stability**.

For all of the measurement points except measurement point 2, the standard deviation of IMEP could be lowered by a small number of control interventions.

Table 5. Control results at different measurement points and n = 1500 1/min

Measurement Point	Load / bar		σIMEP / bar		IMEP peak-peak / bar		Control-Interventions / -	Impr. of σIMEP / %	Impr. of peak-peak / %
DCA	Off	On	Off	On	Off	On			
1	1.67	1.68	0.37	0.35	2.85	2.16	3/250	2.93	24.21
2	1.78	1.77	0.31	0.32	2.29	1.77	3/250	-3.38	22.71
3	1.83	1.85	0.35	0.31	2.23	1.67	2/250	10.77	25.11
4	1.84	1.86	0.31	0.29	1.64	1.63	2/250	3.79	0.61
5	1.83	1.83	0.38	0.31	5.58	1.87	4/250	16.83	66.49
6	1.77	1.72	0.30	0.20	1.32	0.79	32/200	34.65	39.88
7	1.67	1.69	0.35	0.21	1.54	0.68	18/200	39.21	56.15
8	1.78	1.78	0.20	0.19	1.35	0.79	9/200	8.63	41.77
9	1.69	1.75	0.26	0.19	1.10	0.77	5/200	26.34	30.02
10	1.74	1.77	0.24	0.17	1.03	0.78	3/200	27.72	24.14

However, the lowering of the deviation between maximum and minimum IMEP is even more interesting. Here, significant improvement was achieved by the control algorithm even for measurement point 2. Extreme outliers were minimized by only considering a very limited number of actuated cycles.

The effectiveness of the DCA depends mainly on the accuracy of the calculation of $m_{\text{fuel,res}(i-1)}$. Whereas the heat release due to pressure and volume change is easy to calculate with very little use of the resources of the FPGA, there can be uncertainties in the wall heat model as well as the injector model.

Conclusion and Outlook

The presented work analyzes the occurrence of significant combustion patterns and IMEP as well as heat release overshoots after incomplete combustions in GCAI combustion **with internal exhaust gas recirculation**. Residual fuel is found to be one major factor affecting the combustion of the subsequent cycle. Incomplete combustion was found to be a trigger for unstable sequences. Autocorrelation diagrams were used to identify boundaries where control interventions could stabilize GCAI. This coupling of consecutive cycles and the subsequent overshoot was observed especially at load points below 2 bar IMEP.

The IMEP of subsequent cycles was predicted based on the residual fuel. A good accordance between the prediction and the measurement results was found. **Further development of the control algorithm will add a calculation of κ to improve the prediction results.**

The presented control algorithm analyzes the heat release and the amount of residual fuel in real time to adapt the injection duration accordingly and stabilize the combustion.

The initial experimental results were obtained for low load operation, where the low exhaust gas enthalpy does not allow a complete conversion of the residual fuel during intermediate compression. The results show the potential for real-time adaptation of the injected fuel mass within the combustion cycle. It was possible to decouple critical combustion cycles and stabilize the combustion process. The standard deviation of IMEP could be lowered at most of the measurement points.

However, further improvement and testing of the control algorithm are necessary. The offline calculation and calibration of the residual gas fraction will be replaced by a real time gas exchange calculation, enabling the controller to be independent of simulation accuracy.

The online calculation of the heat release can further be used to trigger other control interventions, such as additional water injection **or spark assistance. To increase control variability the decoupling control algorithm can also be brought together with a control of the negative valve overlap.**

Acknowledgments

This work was performed in preparation of the research group 2401, funded by DFG (Deutsche Forschungsgemeinschaft).

This work was partially performed within the „Center for Mobile Propulsion“, which is funded by the Deutsche Forschungsgemeinschaft(DFG).

References

1. Lehrheuer B, Morcinkowski B, Pischinger S et al. Low Temperature Gasoline Combustion – Potential, Challenges, Process Modeling and Control. *Active flow and combustion control 2014: Notes on Numerical Fluid Mechanics and Multidisciplinary Design* 2014; DOI:10.1007/978-3-319-11967-011.
2. Jakob Andert. *Modellbasierte Echtzeitoptimierung der ottomotorischen Selbstzündung*. RWTH Aachen University, 2012.
3. Davis L. Controlling Cyclic Combustion Variations in Lean-Fueled Spark-Ignition Engines. *SAE 2001 World Congress* 2001; DOI:10.4271/2001-01-0257.
4. Rezaei J, Shahbakhti M, Bahri B et al. Performance prediction of HCCI engines with oxygenated fuels using artificial neural networks. *Applied Energy* 2015; DOI:10.1016/j.apenergy.2014.10.088.

5. Ma H, Xu H, Wang J et al. Model-Based Multiobjective Evolutionary Algorithm Optimization for HCCI Engines. *IEEE Transactions on Vehicular Technology* 2015; DOI:10.1109/TVT.2014.2362954.
6. Langen P, Melcher T, Missy S et al. Neue BMW Sechs- und Vierzylinder-Ottomotoren mit High Precision Injection und Schichtbrennverfahren. *28th International Vienna Motor Symposium* 2007; .
7. Kulzer A, Fischer W, Karrelmeyer R et al. Kontrollierte Selbstzündung beim Ottomotor CO2 Einsparpotenziale. *MTZ - Motortechnische Zeitschrift* 2009; DOI:10.1007/BF03225457.
8. Waltner A, Lückert P, Schaup U et al. Die Zukunftstechnologie des Ottomotors: strahlgeführte Direkteinspritzung mit Piezo-Injektor. *27th International Vienna Motor Symposium* 2006; .
9. Vaughan A and Bohac SV. An Extreme Learning Machine Approach to Predicting Near Chaotic HCCI Combustion Phasing in Real-Time. *Preprint* 2013; .
10. Lehrheuer B, Pischinger S, Wick M et al. A Study on In-Cycle Combustion Control for Gasoline Controlled Autoignition. In *SAE 2016 World Congress and Exhibition*. SAE Technical Paper Series, SAE International400 Commonwealth Drive, Warrendale, PA, United States. DOI:10.4271/2016-01-0754.
11. Bahri B, Aziz AA, Shahbakhti M et al. Understanding and detecting misfire in an HCCI engine fuelled with ethanol. *Applied Energy* 2013; DOI:10.1016/j.apenergy.2013.03.004.
12. Hellström E, Stefanopoulou A, Vavra J et al. Understanding the Dynamic Evolution of Cyclic Variability at the Operating Limits of HCCI Engines with Negative Valve Overlap. *SAE International Journal of Engines* 2012; DOI:10.4271/2012-01-1106.
13. Hellström E, Larimore J, Stefanopoulou A et al. Quantifying Cyclic Variability in a Multicylinder HCCI Engine With High Residuals. *Journal of Engineering for Gas Turbines and Power* 2012; DOI:10.1115/1.4007164.
14. Hellstrom E, Stefanopoulou AG and Li Jiang. Cyclic Variability and Dynamical Instabilities in Autoignition Engines With High Residuals. *IEEE Transactions on Control Systems Technology* 2013; DOI:10.1109/TCST.2012.2221715.
15. Pfluger J, Andert J, Ross H et al. Rapid Control Prototyping for Cylinder Pressure Indication. *MTZ - Motortechnische Zeitschrift* 2012; DOI:10.1007/s35146-012-0503-2.
16. Günter Hohenberg. *Experimentelle Erfassung der Wandwärme in Kolbenmotoren*. 1980.
17. Chang J, Güralp O, Filipi Z et al. New Heat Transfer Correlation for an HCCI Engine Derived from Measurements of Instantaneous Surface Heat Flux. In *2004 Powertrain & Fluid Systems Conference & Exhibition*. SAE Technical Paper Series, SAE International400 Commonwealth Drive, Warrendale, PA, United States. DOI:10.4271/2004-01-2996.
18. Jade S, Larimore J, Hellstrom E et al. Controlled Load and Speed Transitions in a Multicylinder Recompression HCCI Engine. *IEEE Transactions on Control Systems Technology* 2015; DOI:10.1109/TCST.2014.2346992.
19. Morcinkowski B, Ewald J, Adomeit P et al. Numerical investigation of cycle-to-cycle fluctuations at gasoline controlled auto-ignition engines. *Fisita World Congress* 2014; (RWTH-2015-02939).
20. Jungkunz AF, Erlien S and Gerdes JC. Late phasing homogeneous charge compression ignition cycle-to-cycle combustion timing control with fuel quantity input. *2012 American Control Conference - ACC 2012* 2012; DOI:10.1109/ACC.2012.6315249.
21. Xilinx I. *7 Series FPGAs Configurable Logic Block: User Guide*. Xilinx, 2014.